Environment and Natural Resources Journal

Volume 22
Issue 4
2024

Biomass and Carbon Stock Estimation through Remote Sensing and Field Methods of Subtropical Himalayan Forest under Threat Due to Developmental Activities

Vivek Dhiman[1,2] and Amit Kumar[1*]

[1]RS-GIS Laboratory, Environmental Technology Division, CSIR-Institute of Himalayan Bioresource Technology, Palampur, Himachal Pradesh-176 061, India

[2]Academy of Scientific and Innovative Research (AcSIR), Ghaziabad- 201002, India

ARTICLE INFO

Received: 29 Jan 2024
Received in revised: 8 Jul 2024
Accepted: 11 Jul 2024
Published online: 25 Jul 2024
DOI: 10.32526/ennrj/22/20240018

Keywords:
REDD+/ Regional climate/ Forest restoration/ Policymaking

*** Corresponding author:**
E-mail: amitkr@ihbt.res.in

ABSTRACT

Mixed subtropical forests possess a high amount of carbon pool owing to their rich species diversity and carbon sequestration potential. The Dhaulasidh forest is located in Himachal Pradesh within the subtropical Himalayan region. This research aimed to identify: (1) Optimal satellite-derived Sentinel-2A indices for predicting biomass, (2) the best-fitting model for biomass estimation, and (3) changes in above-ground carbon stock due to biomass loss, using satellite remote sensing and quadrat-based approaches. Results indicated that Band 3 (Green), Band 5 (Red edge), the vegetation (VEG) index, and the Carotenoid reflectance index (CRI) were suitable for estimating above-ground biomass (AGB). Shannon and Simpson's diversity indices were calculated as 0.89 and 0.73, respectively. Significant contributors to AGB included *Mallotus philippensis*, *Emblica officinalis*, *Cassia fistula*, *Acacia catechu*, *Ehretia laevis*, *Kydia calycina*, and *Lannea coromandelica*. The AGB prediction model based on vegetation indices demonstrated a strong correlation between observed and predicted biomass (R^2=0.65, $p<0.001$), with a mean absolute percentage error of 20% and root mean square error of 7.33 tonnes per pixel. The study predicted a total loss of 22,917.15 tonnes of CO_2 in mixed subtropical forests, representing a 12.04% reduction in carbon stock within the study area. These findings offer critical baseline data for environmental management and carbon balance in the forest ecosystem, recommending that forest management practices after deforestation should be reviewed for remedial measures for any developmental activities.

1. INTRODUCTION

The estimation of carbon loss is a crucial element for national carbon accounting. The United Nations Framework Convention on Climate Change (UNFCCC) recommends that developing countries should adhere to the Intergovernmental Panel on Climate Change (IPCC) protocol for CO_2 emission estimation (UNFCCC, 2009). Preparation of a parametric model for measuring these changes requires the collection of plot-level activity data, such as forests under degradation, carbon loss into the atmosphere due to forest degradation, and forests required to be monitored after degradation. This information may be retrieved from forest inventory data and remote sensing techniques. Forest degradation can be attributed to the loss of carbon stock within forest land (UNFCCC, 2008), mostly due to deforestation (Peres et al., 2006). To a larger extent, forest degradation contributes to 12-20% of greenhouse gas (GHG) emissions globally (CFU, 2020). Pearson et al. (2017), estimate that due to annual forest degradation, 2.1 billion tonnes of CO_2 were emitted across developing countries. From various anthropogenic activities, about 10.34% of the global forest cover was lost between 1990 and 2020 (Lousada et al., 2022). In Euthopia, Moisa et al. (2023), reported that from 1992 to 2022, forest degradation resulted in a

Citation: Dhiman V, Kumar A. Biomass and carbon stock estimation through remote sensing and field methods of subtropical Himalayan Forest under threat due to developmental activities. Environ. Nat. Resour. J. 2024;22(4):378-393. (https://doi.org/10.32526/ennrj/22/20240018)

decline in the carbon stock of 58,883.4 tonnes/km^2, and the past three decades exhibited 2,418,083.91 tonnes of carbon emission annually.

The functioning of the ecosystem is influenced by the change in regional biomass due to forest degradation as per the Reducing Emissions from Deforestation and Forest Degradation (REDD+) programme. The biomass changes are a combination of five carbon pools: above-ground biomass (AGB), below-ground biomass, soil organic matter (SOM), deadwood, and litter (IPCC, 2003). Among these, AGB accounts for CO_2 emitted due to deforestation, ultimately responsible for climatic changes (Lu et al., 2005). Carbon losses exert a substantial impact on ecosystems, posing significant threats to ecological stability and function, underscoring the critical need for evaluation (Lingbing and Jing, 2022). Research on land-use carbon emissions primarily focuses on carbon emission accounting (Luo et al., 2024; Zhang and Zhang, 2023) and low-carbon optimisation (Yan et al., 2023). In these scenarios, accurate estimation of AGB loss is central for precise quantification of CO_2 emission.

Initially, species-specific allometric equations were used for AGB estimation (Navar, 2009; Pearson et al., 2005). Allometric equations estimate biomass using parameters measured from trees (e.g., height, diameter at breast height (DBH), and wood density). These equations establish a scaling relationship between tree form and function to predict total biomass (West et al., 1999). Later, remote sensing technology gained attention for forest biomass estimation after the launch of resource-monitoring satellites (Lu et al., 2016). Consequently, allometric equations derived from the field, along with modelled remote sensing equations, were used for AGB and carbon stock estimation in forest ecosystems (Brown, 1993; Vashum and Jayakumar, 2012).

Remote sensing-based methods are widely utilised for AGB estimation due to their advantages, such as the repeatability of data collection and high correlations between spectral bands and vegetation parameters. However, selecting the spatial resolution of data is crucial as it influences the performance of image texture and discrimination of land covers, especially in complex forest stand structures (Lingbing and Jing, 2022).

According to Houghton et al. (2009), satellite missions provided the opportunity for measurement and mapping of biomass and carbon emission changes on local to global scales. Data retrieved from satellite sensors were used in measurements of different vegetation traits estimations such as the leaf area index, tree density, tree volume, tree crown size, and tree height. These traits are used in biomass estimation (Isbaex and Coelho, 2021). Information derived from the amalgamation of quadrats laid in the forest with remote sensing images is widely used in forest studies (Chen et al., 2019), embedding predictive models for monitoring AGB and carbon estimation (Castillo et al., 2017). Satellite images provide varied spatial, temporal, and spectral resolutions (Timothy et al., 2016). Low spatial resolution images with broad bandwidth were found inappropriate for AGB estimation of subtropical forests consisting of high species diversity (Mutanga and Skidmore, 2004; Pandit et al., 2018) and require high spatial resolution, narrow-bandwidth spectral images that provide comparatively more accurate AGB estimation.

The multispectral sensor of Sentinel 2 is the types of high spatial resolution (<10 m) images that are resampled to match sample plot field data. Thus, vegetation indices (VI), spectral bands, and biophysical variables (Isbaex and Coelho, 2021; Zhang et al., 2017) derived from Sentinel images can improve the accuracy of AGB predictor models. Sentinel 2 images are freely accessible at the European Space Agency (ESA) hub (Zhang et al., 2017). Chrysafis et al. (2017), found a significant relationship between growing stock volume and VI (R^2=0.63; RMSE of 63.11 m^3/ha) of Sentinel 2 MSI imagery for the heterogeneous forest in northeastern Greece. Accurate biomass estimation is crucial for analysing the impact of deforestation on regional environmental degradation in the global climate change scenario. Biomass loss estimation is also important to meet compensation actions of the REDD+ programme and the net-zero carbon emission plan of UNFCCC. These targets can be achieved using Sentinel 2 imagery, which provides an opportunity for improved and accurate AGB estimation with modelling of image-driven VI and field-measured vegetation traits (Castillo et al., 2017).

In the above background, we aimed to find Sentinel-derived best predictive indices for biomass estimation, the best-fitting model for biomass estimation, and changes in carbon stock in terms of AGB loss in the study area.

2. METHODOLOGY

2.1 Study area

Dhaulasidh is part of the subtropical Himalayan forest located at 31.80477 N latitude and 76.43964 E longitude in the Hamirpur District of Himachal Pradesh, India (Figure 1). Annual mean temperature and rainfall of the region vary from 17.96 to 27.9°C and 42.86 mm, respectively. A total of 142.6 ha area is under forest cover, having an elevation of 469-869 m AMSL. A 66W hydel power project is proposed to build on Beas River flowing in the study area. This hydel project will generate hydroelectricity and will add 304 million units of energy to the national budget. It will provide irrigation facilities to over 200 village surroundings. Worldwide hydroelectric projects contribute to approximately 16% of global electricity (IHA, 2024). For developing countries, these renewable sources are crucial to meet energy demands, but at the same time, environmental loss due to the hydel projects need to be taken care. For dam construction, a connecting road, and related infrastructure of this hydel project, tree felling was permitted by the local Himachal Pradesh government. It is assumed that approximately 10,000 trees were cut in this exercise (SIAU, 2019).

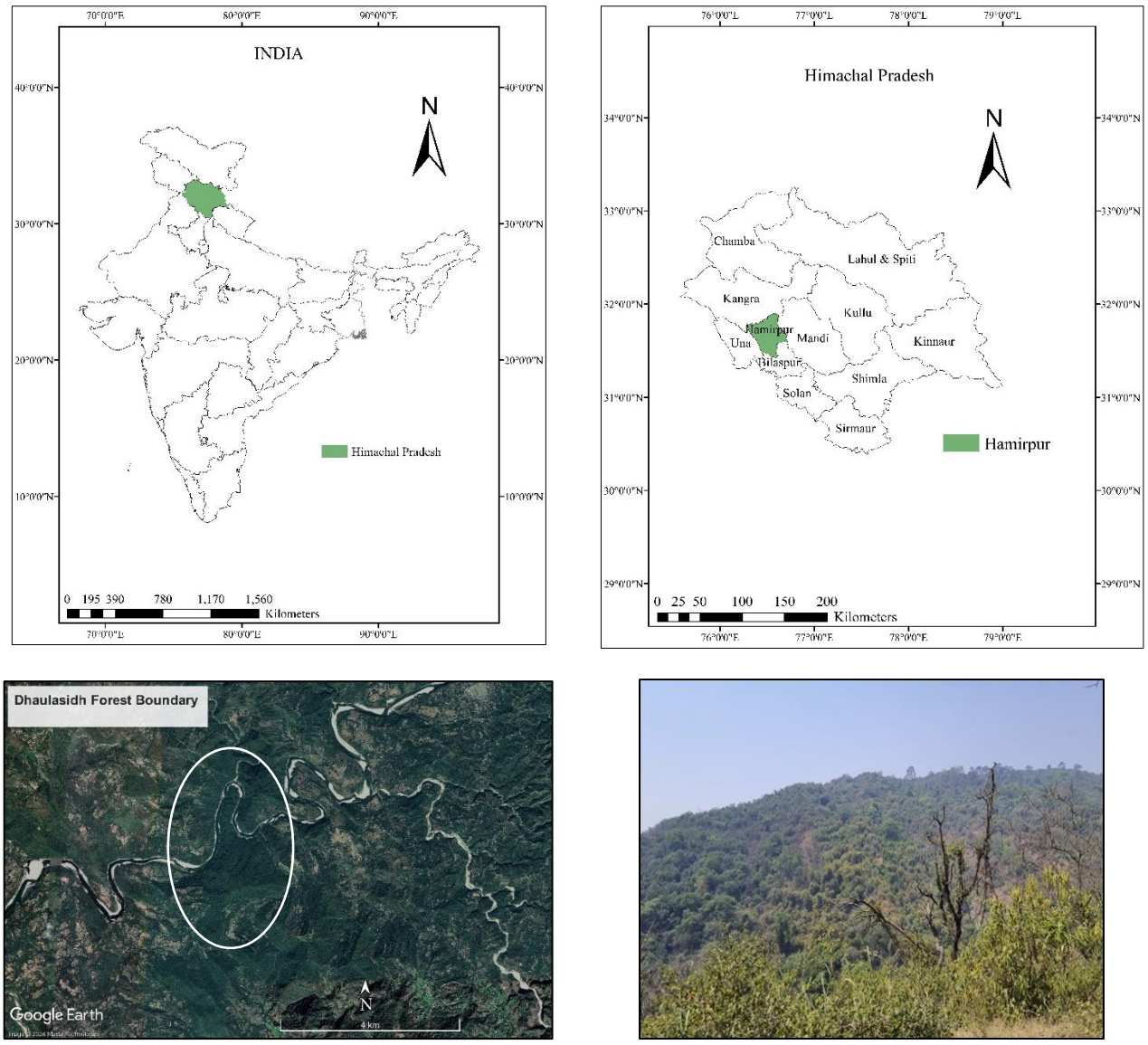

Figure 1. (a) Study area located on country map, (b) state map, (c) Google Earth imagery, and (d) in the field

2.2 Materials and methods

The overall methodology for estimating AGB of the Dhaulasidh forest is shown in Figure 2. An extensive field survey was conducted before the start of tree felling on 15-16 March 2021. A total of 15 quadrats (10×10 m) were established at 300-m

intervals to adequately represent the tree felling area (Figure 3). The geographical coordinates of each plot were recorded using a handheld Global Positioning System device. The DBH of each tree was measured using a tape measure, and tree height was measured using a clinometer. Soil samples from the study area were collected and analysed for nutrient availability, including nitrogen, phosphorus, potassium, and SOM.

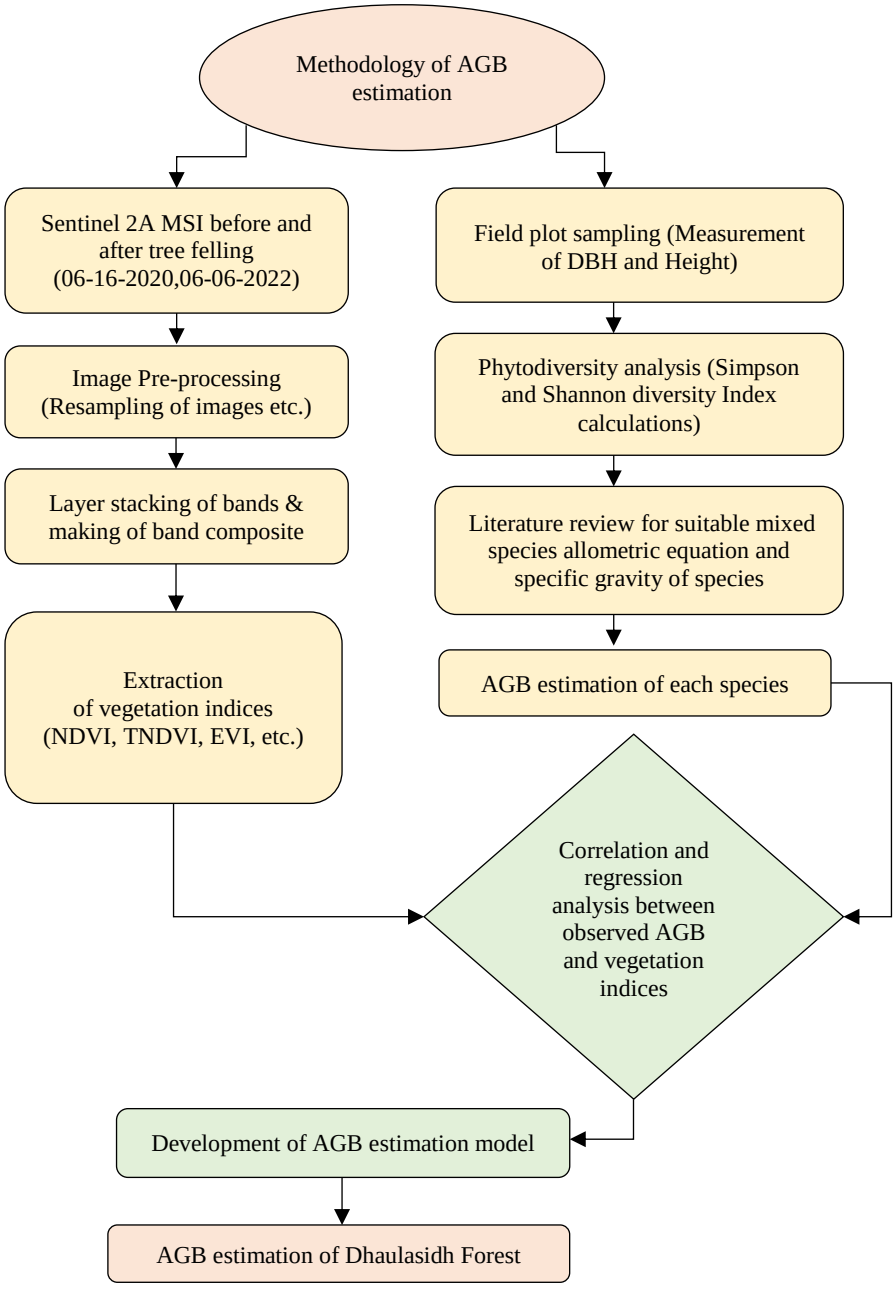

Figure 2. Flow diagram of the methodology for the biomass estimation

Before tree felling, Sentinel-2A MSI image Level-1C (16 June 2020) of the study area was acquired from the ESA for AGB estimation. Raw images were downloaded and pre-processed in the Sentinel Application Platform (SNAP) software, containing 13 spectral bands with spatial resolutions of 20 m and 60 m. In the radiometric correction process, the raw Digital number (DN) values of the Level1-C product were converted into Top of Atmosphere (TOA) radiance using sensor-specific calibration coefficients provided in the metadata. Subsequently, TOA radiance was converted to TOA reflectance. Additionally, the data required resampling and subsetting to match the field variables. Therefore, in the geometric correction method of SNAP, the radiometric corrected images were resampled to 10-m resolution to match the size of the field quadrats. Sentinel images (6 July 2022) were used for AGB loss

estimation after tree felling. Using the supervised classification method, these satellite images were classified (Figure 4) in Erdas Imagine software version 16, and the land cover map was prepared. The training dataset for classification was identified through visual image interpretation. The maximum likelihood parametric decision rule was applied to image pixels and the land cover map prepared, resulting in forest classes mixed with open/barren lands. Forest canopy cover >70% was categorised as very dense forest, 50-70% as dense forest, 40-50% as moderately dense forest, 10-40% as open forest, and <10% canopy cover as scrub forest (Farooq and Rashid, 2010).

Figure 3. 10×10-meter quadrat-based vegetation sampling in the study area

The accuracy of the classified image was assessed using sensitivity, specificity, and true skill statistical (TSS) analysis in the R software package. A 2×2 confusion matrix was applied to the classified images to determine true positives (a), false positives (b), false negatives (c), and true negatives (d) using Equations (1-3) (Allouche et al., 2006).

$$\text{Sensitivity} = \frac{a}{a+c} \quad (1)$$

$$\text{Specificity} = \frac{d}{b+d} \quad (2)$$

$$\text{TSS} = \text{Sensitivity} + \text{Specificity} - 1 \quad (3)$$

The phytodiversity of the study area was calculated using Simpson (Simpson, 1949) and Shannon-Weiner Indices (Shannon and Weaver, 1949) using Equations 4 and 5. The Simpson diversity index measures the presence and abundance of species in their habitat, while the Shannon-Weiner index measures uncertainty of the species and community diversity. Lower uncertainty indicates lower community diversity and vice versa.

$$\text{Simpson diversity index (D)} = 1/\sum_{i=1}^{s} p_i^2 \quad (4)$$

Where; p = proportion (n/N) of individuals of one particular species (n) divided by total number of individuals (N), Σ is the sum of the calculations, and s=number of species.

$$\text{Shannon-Weiner Index (H)} = -\sum_{i=1}^{s} p_i \ln p_i \quad (5)$$

Where; p=proportion (n/N) of individuals of one particular species (n) divided by the total number of individuals (N), ln is natural log, Σ is the sum of the calculations, and s=number of species.

Global, regional, and local biomass estimations are influenced by the choice of biomass estimation equation. Therefore, the selection of an equation is

crucial as it affects accuracy when applied with remote sensing data for regional biomass prediction (Mitchard et al., 2013). Several allometric equations are available for AGB estimation (Chaturvedi and Raghubanshi, 2013; Rawat and Singh, 1988); among them, the equation proposed by Nath et al. (2019), (Equation 6) was considered the most accurate for AGB estimation of mixed woody species and was used in this study.

$$AGB\ (kg/m^3) = 0.32*p*D\text{^}2* H\text{^}0.75 *1.34 \quad (6)$$

Where; p=wood density, D=diameter at breast height, H=height.

Wood density or wood specific gravity (WSG) is an important factor in forest biomass calculations (Fearnside, 1997). It represents the density of oven-dried wood relative to water density and varies between species due to water content differences (Kuyah et al., 2012; Mukuralinda et al., 2021). In this study, WSG values for plant species (Table 1) were obtained from a subtropical species-based wood density database (Reyes, 1992) and literature on Himalayan woody species. These WSG values were used for quadrat-wise AGB estimation (Equation 6).

The carbon stock of the study area was calculated using Equation 7 by multiplying biomass with a carbon fraction value of 0.47 (IPCC, 2006).

$$C = AGB \times CF \quad (7)$$

Where; C=carbon stock, CF=carbon fraction value.

A review of literature was conducted to identify spectral VI used in biomass estimation (Table 2). These indices were calculated for Sentinel images before tree felling. The shapefile of the quadrat overlaid on the spectral vegetation index image allowed the retrieval of indices for each quadrat. An AGB prediction model was developed by correlating spectral VI with biomass for each quadrat. This model was applied to the Sentinel image of the study area for regional biomass estimation.

Table 1. Various wood specific gravity values used in the present study

Serial No.	Species with wood specific gravity values	Source
1	*Bauhinia veriegata*=0.59, *Lannea coromandelica*=0.46, *Bombax malabaricum*=0.33, *Casearia elliptica*=0.64, *Toona ciliata*=0.55, *Ehretia laevis*=0.56, *Melia azedarach*=0.69, *Acacia catechu*=0.77, *Ficus auriculata*=0.44, *Dalbergia sissoo*=0.68, *Cassia fistula*=0.81, *Ougeniao ojeinensis*=0.60, *Grewia optiva*=0.71, *Syzygium cumini*=0.66, *Mallotus philippinensis*=0.64, *Emblica officinalis*=0.61	Sheikh et al. (2011)
2	*Terminalia chebula*=0.96, *Kydia calycina*=0.72, *Crataeva religiosa*=0.53, *Albizia lebbeck*=0.55, *Zanthoxylum rhetsa*=0.33	Reyes (1992)
3	*Ehretia laevis*=0.56, *Eugenia jambolana* Lam.=0.89	ICRAF (2007)
4	*Ficus religiosa* L.=0.51, *Ziziphus mauritiana*=0.49	Bisleshna et al. (2019)

Table 2. Spectral vegetation indices for biomass estimation used in the present study

Vegetation Indices	Formula	Reference
Woebbecke index (WI)	G–B/R–G	Woebbecke et al. (1995)
Normalized Difference Vegetation Index (NDVI)	(NIR–R)/(NIR+R)	Rouse et al. (1974)
Wide Dynamic Range Vegetation Index (WDRVI)	(0.1*NIR–R)/(0.1*NIR+R)	Gitelson (2004)
Colour Index of Vegetation (CIVE)	0.441*R0.881*G+0.385*B+18.78745	Kataoka et al. (2003)
Vegetative (VEG)	$G/(R^aB^{(1-a)})$; a= 0.66	Marchant and Onyango (2000)
Excess Green Index (ExG)	2*G–R –B	Woebbecke et al. (1995)
Visible Atmospherically Resistant Index (VARI)	G–R/G+R–B	Gitelson et al. (2003)
Excess Green minus Excess Red (ExGR)	ExG –1.4*R – G	Meyer and Neto (2008)
Ratio Vegetation Index (RVI)	NIR/R	Pearson and Miller (1972)
Green Leaf Index (GLI)	2*G–R–B)/(2*G+R+B)	Hunt et al. (2011)
Normalized Green Red Difference Index (NGRDI)	G–R/G+R	Gitelson et al. (2002a)
Carotenoid Reflectance Index (CRI)	$1/R_G+1/R_{NIR}$	Gitelson et al. (2002b)

Table 2. Spectral vegetation indices for biomass estimation used in the present study (cont.)

Vegetation Indices	Formula	Reference
Transformational Vegetation Index(TVI)	$\sqrt{NDVI + 0.5}$	Broge et al. (2001)
SAVI (Soil-Adjusted Vegetation Index)	$(R_{NIR}–R_R)/(R_{NIR}+R_R+0.5)\times1.5$	Huete (1988)
Optimized Soil-Adjusted Vegetation Index (OSAVI)	$(R_{NIR}–R_R)/(R_{NIR}+R_R+1.6)\times1.16$	Rondeaux et al. (1996)
Green-NDVI (GNDVI)	$(R_{NIR}–R_G)/(R_{NIR}+R_G)$	Gitelson (1996)
Ratio Vegetation Index (RVI)	R_{NIR}/R_R	Baret et al. (1991)
Enhanced Vegetation Index (EVI)	$2.5\times(R_{NIR}–R_R)/(1+R_{NIR}+6\times R_R–7.5\times R_B)$	Liu and Huete (1995)
Modified Simple Ratio Index (MSR)	$((R_{NIR}/R_R)–1)/\sqrt{R_{NIR}/R_R + 1}$	Chen (1996)
Nonlinear Vegetation Index (NLI)	$(R_{NIR}\times R_{NIR}–R_R)/(R_{NIR}\times R_{NIR}+R_R)$	Goel and Qin (1994)
Re-normalized Difference Vegetation Index (RDVI)	$(R_{NIR}–R_R)/\sqrt{R_{NIR}+R_R}$	Ke et al. (1998)
Modified Triangular Vegetation Index 2 (MTVI2)	$1.5\times[1.2\times(R_{NIR}–R_G)–2.5\times(R_R–R_G)/\sqrt{2\times(R_{NIR}+1)^2 – 6\times R_{NIR} + 5\times\sqrt{R_R – 0.5}}$	Haboudane et al. (2004)

3. RESULTS

Analysis of the land cover map of the Dhaulasidh forest before and after deforestation (Figure 4, Figure 5, and Table 3) revealed significant decreases in forest types post-tree felling: a 2.55% decrease in very dense forests (from 196.18 ha in 2020 to 186.06 ha in 2022), 1.25% reduction in dense forests (from 160.26 ha to 155.05 ha), 1.71% decrease in moderately dense forests (from 43.51 ha to 36.43 ha), 0.26% decline in open forests (from 9.56 ha to 8.45 ha), and 0.29% reduction in barren land (from 6.23 ha to 5.02 ha).

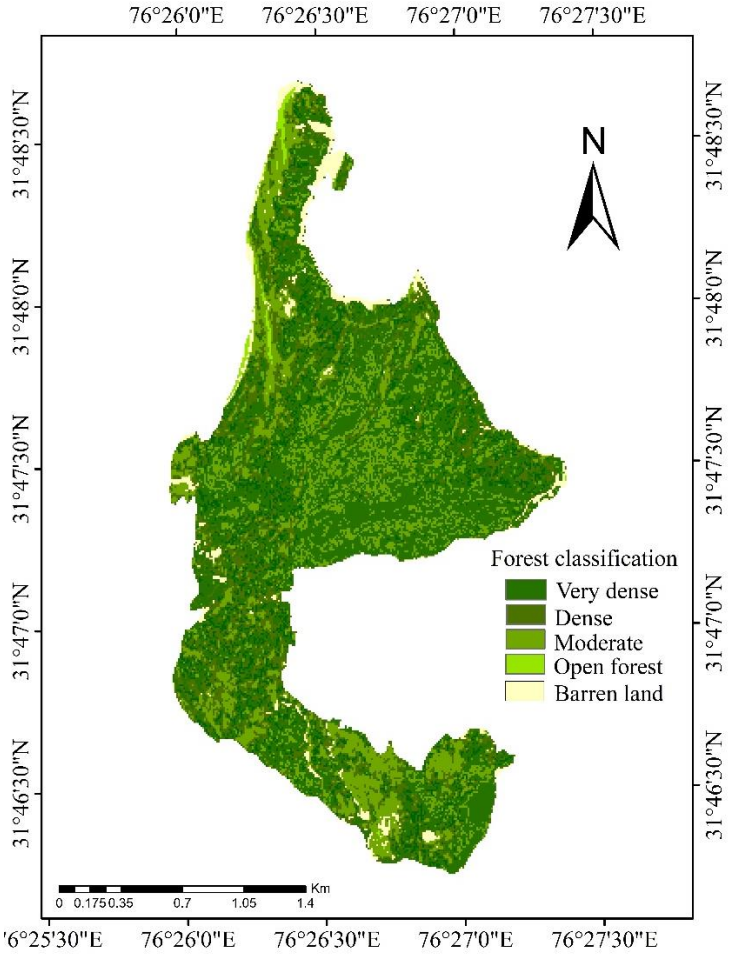

Figure 4. Classified land cover map of 2020 of the study area before tree felling

Table 3. Forest type and representation area of land cover map of 2020 before tree felling

Land cover type	2020 before tree felling area (ha)	2022 after tree felling area (ha)	Change (%)
Very dense forest	196.18	186.06	-2.55%
Dense forest	160.26	155.05	-1.25%
Moderately dense forest	43.51	36.43	-1.71%
Open forest	9.56	8.45	-0.26%
Barren land	6.23	5.02	-0.29%

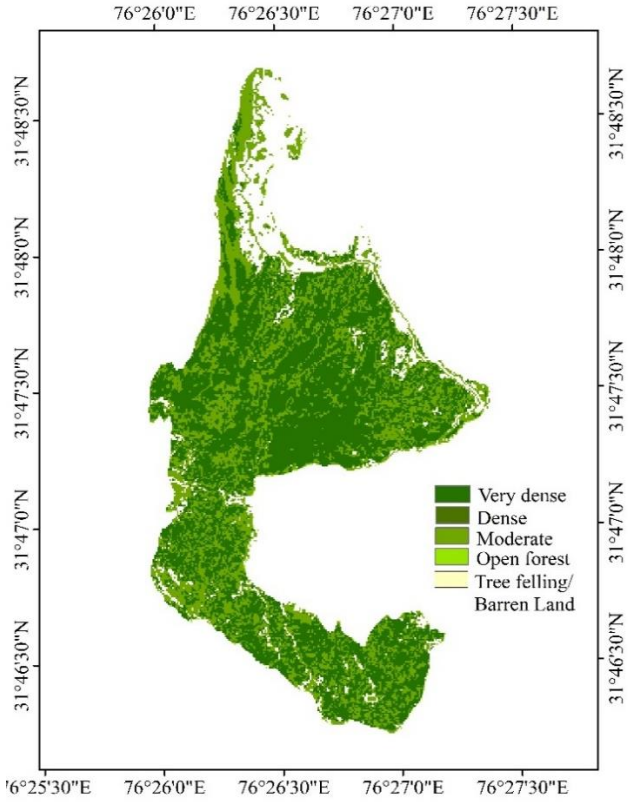

Figure 5. Classified land cover map of 2022 of the study area after tree felling

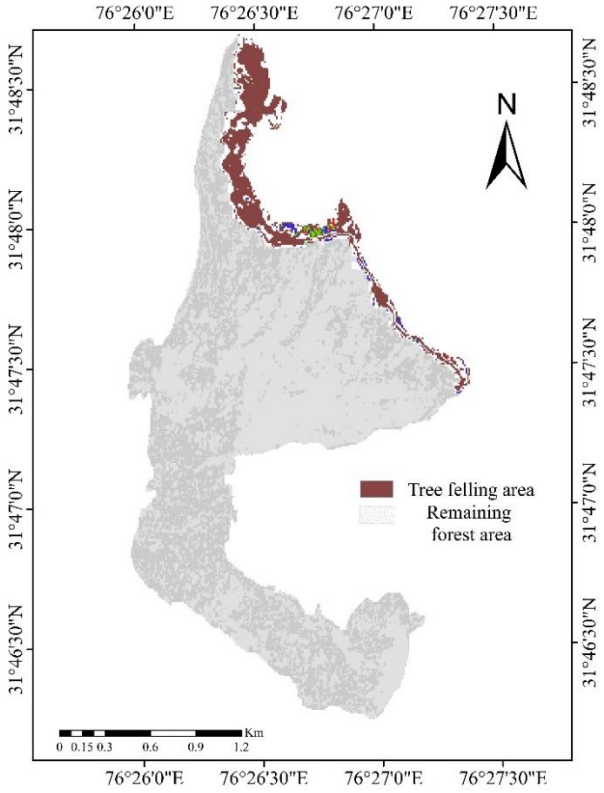

Figure 6. Forest area underwent tree felling for hydel project

The accuracy assessment of the classified image provided sensitivity, specificity, and TSS values of 0.8633, 0.9420, and 0.8059, respectively. It was unaffected by the occurrence and size of the validation set (Allouche et al., 2006), calculated commission and omission errors, and assessed results ranging from –1 to +1, where +1 indicates ideal agreement and values towards 0 and below indicate poorer results.

3.1 Quadrat-wise AGB

The quadrat-wise AGB of the Dhaulasidh forest was estimated (Table 4) using Equation 6 with WSG values (Table 1) of individual species. The 13th quadrat had the lowest AGB (2.56 tonnes/ha), whereas the 5th quadrat had the highest AGB (25.5 tonnes/ha). Phytodiversity analysis found Simpson diversity index (D) ranging from 0 to 0.89 and Shannon-Weiner Index (H) from 0 to 0.73. The 2nd quadrat showed zero diversity due to dominance by *Mallotus philippinensis*. The 9th quadrat possessed the highest species diversity, hosting six species: *Cassia fistula*, *Bombax malabaricum*, *Emblica officinalis*, *Acacia catechu*, *Mallotus philippinensis*, and *Crataeva religiosa.*

A total of 25 woody species were recorded across 15 quadrats during field surveys. These species were *Ziziphus mauritiana*, *Zanthoxylum rhetsa*, *Mallotus philippinensis*, *Albizia lebbeck*, *Ficus religiosa*, *Syzygium cumini*, *Grewia optiva*, *Ougenia oojeinensis*, *Eugenia jambolana*, *Cassia fistula*, *Emblica officinalis*, *Dalbergia sissoo*, *Mangifera indica*, *Acacia catechu*, *Ehretia laevis*, *Melia azedarach*, *Ficus auriculata*, *Casearia tomentosa*, *Toona ciliata*, *Bombax malabaricum*, *Crataeva*

religiosa, *Kydia calycina*, *Lannea coromandelica*, *Terminalia Chebula*, and *Bauhinia variegata*.

Table 4. Quadrat-wise biomass of the study area

Quadrat No.	Area (m^2)	AGB (ton/ha)
1	100	17.94
2	100	23.04
3	100	7.79
4	100	7.29
5	100	25.5
6	100	6.91
7	100	3.47
8	100	4.93
9	100	2.72
10	100	3.86
11	100	5.83
12	100	15.72
13	100	2.56
14	100	4.33
15	100	12.98

3.2 Derivation of AGB from Sentinel image

Polynomial R^2 values of Sentinel image-based spectral bands and vegetation indices (Table 2) with field-observed AGB ranged from 0.13 to 0.68. Second-order polynomial regression was chosen because AGB values for forest species were nonlinear, and a linear regression model would not provide the best-fit line, limiting prediction accuracy.

Predictive variables Green (Band 3), VNIR (Band 5), VEG, and CRI yielded significant coefficient values (Ostertagova, 2012): R^2=0.59, 0.51, 0.59, and 0.68, respectively (Figure 7). Other indices (EVI, NDVI, NDVI45, NLI, ExG, and GLI) showed lower coefficients of determination R^2=0.18, 0.36, 0.26, 0.41, 0.34, and 0.30. Therefore, insignificant predictive variables were excluded from the regression analysis due to multicollinearity, resulting in high variance in prediction (Chen et al., 2018).

Using significant predictor variables, a polynomial regression model (Equation 8) was developed for AGB prediction. Equation 8 was used to calculate AGB values for individual image pixels, providing AGB estimates for the entire forest area. Over- and underestimated pixels were normalised by assigning the mean value of nearby pixels. The derived AGB map of the Dhaulasidh forest (Figure 9(a)) provided biomass estimates ranging from 8 to 38 tonnes/pixel.

$$AGB = \{(327{,}792\times B3^2-57{,}779\times B3+2{,}551.3) + (12{,}840\times B5^2-24{,}919\times B5+1{,}213.9) + (327{,}792\times VEG^2-57{,}779\times VEG+2{,}551.3) + (3.803\times CRI^2-111.1\times CRI+814.64)\} \quad (8)$$

3.3 Model validation for AGB prediction

For validation of the prediction model, predicted and observed AGB values were plotted on the goodness-of-fit line, showing a strong relation with R^2=0.65 (Figure 8) and multiple R=0.61 (p-value<0.5, i.e., 0.01). Mean absolute percentage error (MAPE) was 20% (RMSE=7.33 tonnes/pixel). A MAPE of 10-20% suggests good prediction (Makridakis et al., 1998) and acceptable accuracy (Lewis, 1982). Using the AGB prediction model (Equation 8), a total of 404,686.51 tonnes of AGB was estimated in the 415.74 ha area of the Dhaulasidh forest before tree felling. Similarly, 355,926.63 tonnes of AGB was estimated after tree felling.

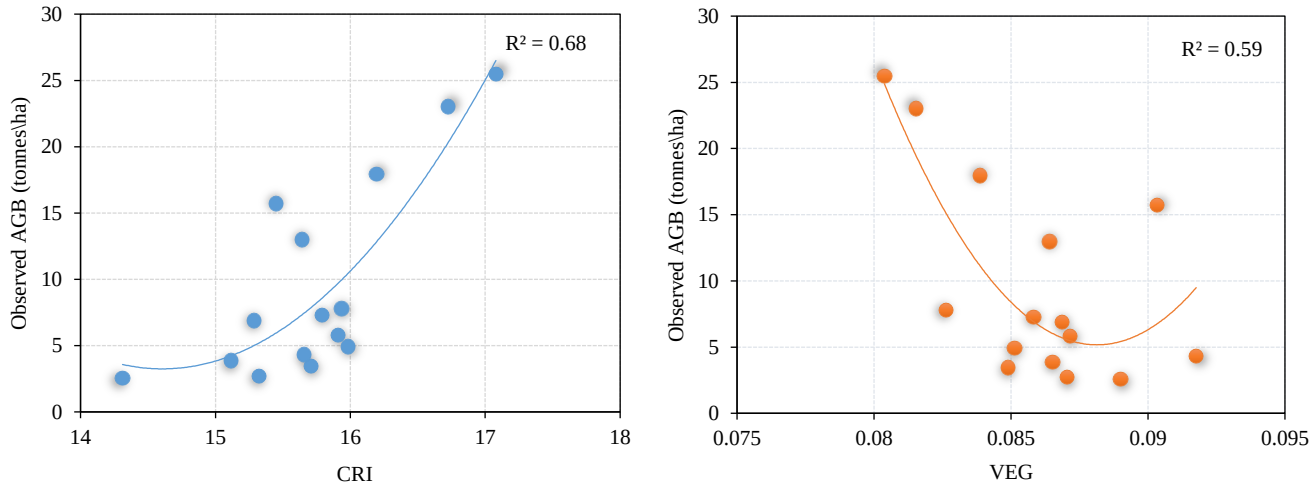

Figure 7. Polynomial regression between spectral values and vegetation indices of image with observed AGB in the field

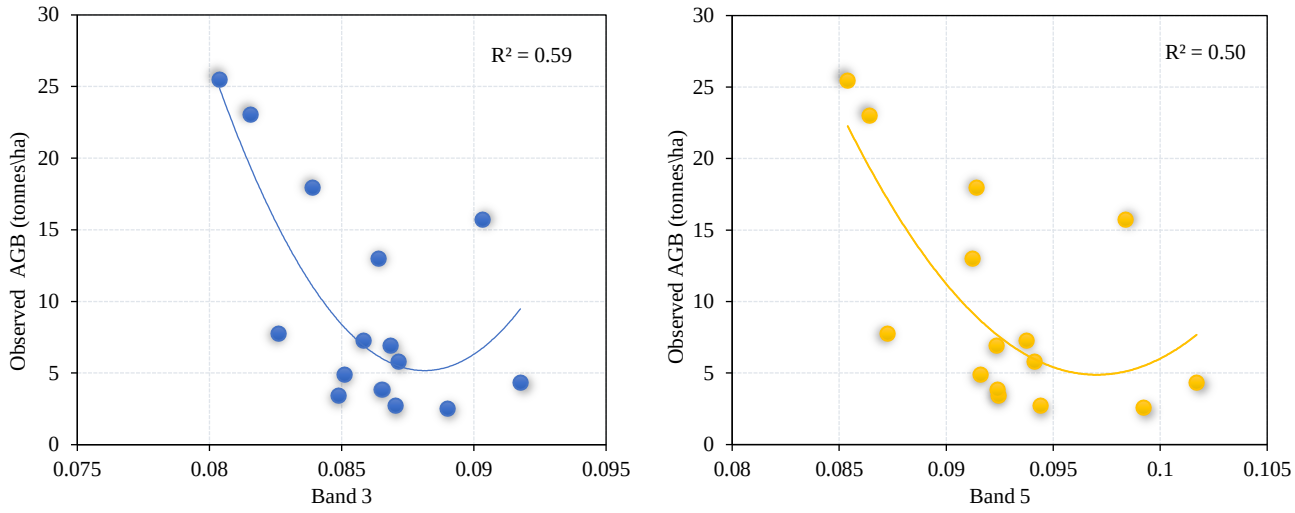

Figure 7. Polynomial regression between spectral values and vegetation indices of image with observed AGB in the field (cont.)

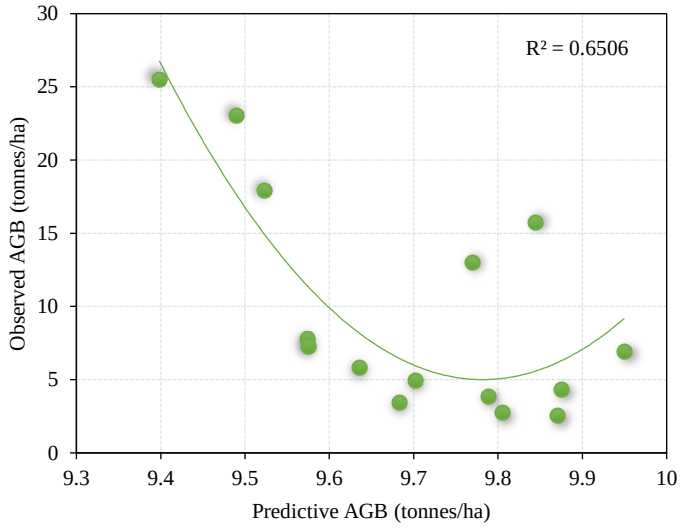

Figure 8. Regression coefficient (R^2) of estimated and observed AGB

3.4 Carbon stock estimation

Using Equation 7 the total above-ground carbon stock was estimated as 190,202.66 C/tonnes/pixel (Figure 9(a)). After tree felling, 167,285.51 C/tonnes/pixel of carbon was estimated. The change in carbon stock of the Dhaulasidh forest was calculated using Equation 9. Thus, a total of 22,917.15 tonnes of carbon loss was estimated due to the tree felling drive for the hydel project in the study area. The obtained results indicate 48,759.88 tonnes of AGB (Figure 9(b)) loss in the Dhaulasidh forest, leading to a reduction in the natural carbon sink. In addition, a total 12.04% loss was observed in AGB and carbon stock of the forest.

Change in carbon stock (ton) = Total Carbon before tree felling – Total carbon after tree felling (9)

4. DISCUSSION

The Green (Band 3) and Red edge (Band 5) bands of Sentinel 2 are efficient in predicting forest-related parameters, including biomass (Astola et al., 2019), which was also found to be significant in our study. The AGB is influenced by the Red edge band due to its presence between high chlorophyll reflectance (red region) and absorption (NIR) regions. The Red edge band, ranging from 680 to 740 nm, reflects the canopy of the forest and is crucial for assessing vegetation and their pigments (Clevers and Gitelson, 2013). Any changes in leaf properties of vegetation can be observed in this region (Slonecker et al., 2009). VEG and CRI indices show a strong

relationship with quadrat AGB, as the reflectance of the Green band strongly influences vegetation indices. Other indices, such as NDVI and EVI, did not show a significant relationship with observed AGB due to pixel saturation caused by high biomass and other factors such as soil, clouds, and atmospheric effects (Nandy et al., 2017).

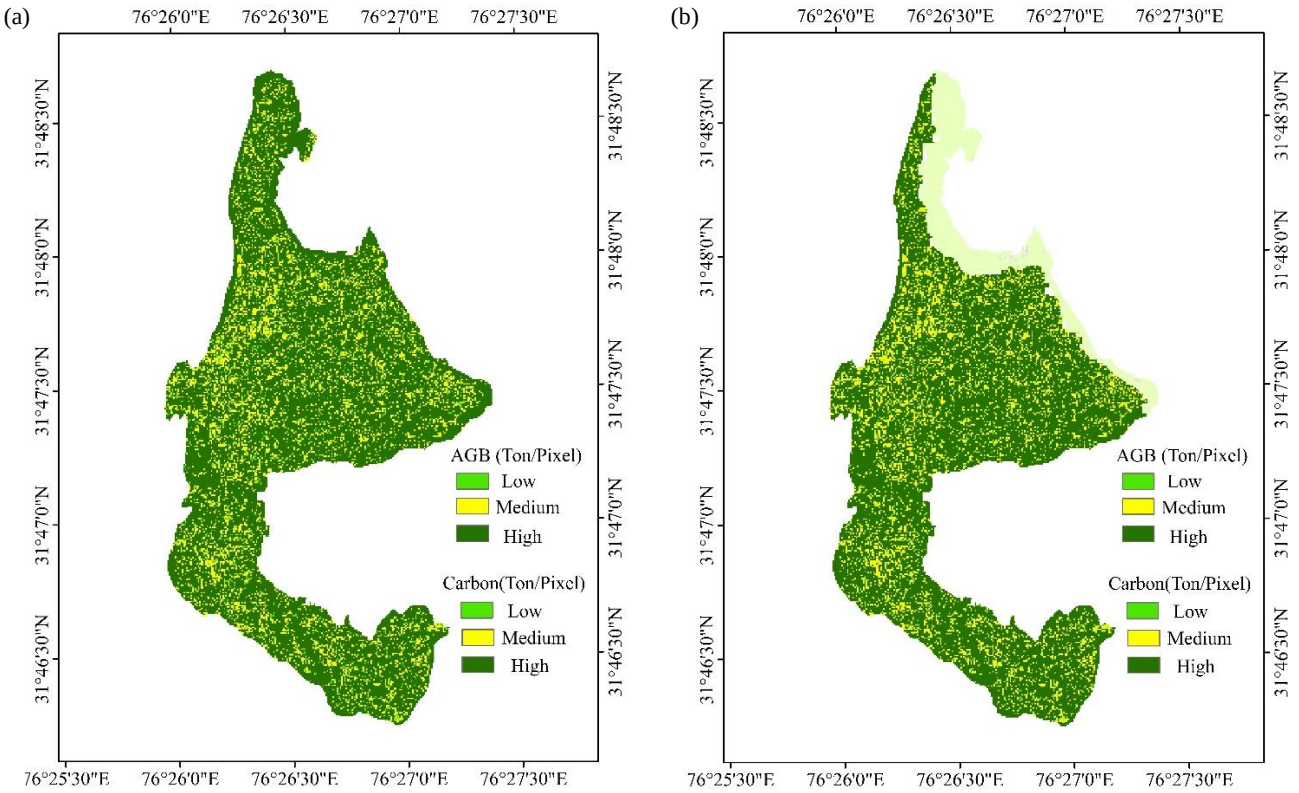

Figure 9. Before and after deforestation AGB and Carbon stock map (a, b) of the study area

The present results of the polynomial model were consistent with those of Ali et al. (2023), where the strongest polynomial regressions of 0.70, 0.70, and 0.72 were observed between AGB and Sentinel 2A-derived indices NDVI, RVI, and ARVI in natural Chir-pine forests. However, a 5% regression value was lower in present study due to the high species diversity in the forest than in mono-plantations. Similar findings for biomass prediction were associated with Lu et al. (2012), indicating that 1st- and 2nd-order polynomial regression models provide accurate prediction results.

While regression models are widely used to analyse factors influencing carbon emissions (Zwane et al., 2023), their integration with diverse space-borne datasets is crucial. This approach not only aids in estimating forest AGB and associated uncertainties but also provides insights into the value of different space-borne datasets, considering coverage area, spatial, and spectral resolution. Such integration allows for biomass estimation in a manner that is both time- and cost-efficient. Khan et al. (2024), examined various remote sensing techniques for estimating forest AGB and found that different forms of regression models are the second most commonly used after random forest models, with varying parameters of space-borne data. Although in the diverse nature of forest environments, it is challenging to identify specific remote sensing datasets, and regression models perform best among others.

The AGB of the study area was calculated as 975 tonnes/hectare, consistent with the AGB range of mixed Himalayan forests at 808.05 tonnes/hectare (Nandy et al., 2017). Species such as *Mallotuss philippensis*, *Emblica officinalis*, *Cassia fistula*, *Acacia catechu*, *Ehretia laevis*, *Kydia calycina*, and *Lannea coromandelica* were found to possess high AGB derived from the quadrat method, similar to findings from the central Himalayan region (Joshi et al., 2021). The mean carbon stock of *Mallotus philippensis* was found to be 0.3473 megagram, and the mean carbon stock of other species was calculated as 0.2350 megagram. The mean basal area was retrieved as 323.1749 square feet/acre for *M.*

philippensis, while for other species, it was 130.39 square feet/acre. The results of Shannon and Simpson diversity analysis, with values of 0.89 and 0.73 respectively, indicate medium to high diversity, underscoring the contribution of mixed species to high AGB in the study area.

Before tree felling, the average AGB of the Dhaulasidh forest was estimated as 9.74 tonnes/pixel, with a minimum of 8.70 tonnes/pixel and a maximum of 38 tonnes/pixel, indicating high AGB levels. After tree felling, the average AGB was observed to be 9.65 tonnes/pixel, with a minimum of 8.70 tonnes/pixel and a maximum of 20.68 tonnes/pixel. AGB ranges were classified as low (8-12 tonnes/pixel), medium (12-16 tonnes/pixel), and high (>16 tonnes/pixel) (Figure 9(a, b)). Soil analysis showed that the soil was highly rich in nutrient contents, with nitrogen ranging from 175.68 to 407.8 kg/ha, phosphorus from 3.96 to 56.13 kg/ha, potassium from 108.03 to 685.66 kg/ha, and SOM from 5.27% to 10.09%. The presence of water bodies within the forest also provides optimal conditions for the growth of the Dhaulasidh forest. These conditions may favour the accumulation of high AGB content.

The study area witnessed mass tree felling (Figure 6), resulting in conditions favourable for an increase in surface albedo, which is the ratio of total radiation reflected from a surface to the total incoming radiation illuminating the surface (Yan et al., 2021). Deforestation influences biogenic volatile organic compounds emitted by forests and affects short-lived climate forcers such as aerosols, ozone, and methane (Scott et al., 2018). Due to deforestation, the incident radiation absorbed by land surfaces may warm the local climate, which needs to be investigated in future studies. While this process is gradual, warming will occur more rapidly in deliberate deforestation scenarios as observed in the present case. Mixed forests promote high biological diversity, carbon storage, and productivity (Nadrowski et al., 2010). Changes in forest cover respond to rainfall patterns and moisture content, affecting evaporative cooling limits due to rainfall (Pitman et al., 2011). The loss of 22,917.15 tonnes of carbon dioxide in the study area due to AGB loss may increase water use efficiency, reducing evapotranspiration (ET). ET is the sum of evaporation from plant surfaces, canopy litter interception, and evaporation from the soil (Baldocchi et al., 2001; Levia et al., 2011). Changes in ET could potentially alter atmospheric moisture content and reduce the local cooling effect (Lawrence et al., 2022), leading to soil erosion and changes in the watershed regime of the forest area. According to Aber and Federer (1992), plant transpiration is closely related to ecosystem productivity and carbon sequestration. Changes in regional climate may influence leaf energy balance, succession stage, morphology stage, and leaf nutrients. A long-term case study of subtropical forests by Zhou et al. (2013), demonstrated that due to temperature rise DBH, height, and biomass of individuals decrease. Also, vegetation shifts are noted as climax communities are replaced by smaller individuals (herbs, shrubs, small trees) due to an imbalance between mortality and recruitment rates. In the Dhaulasidh forest, the invasion of pioneer species over climax species may result from the boundary region of the felling area spreading towards the core zone of the forest. Therefore, species such as *Albizia lebbeck*, *Ficus religiosa*, *Acacia catechu*, *Emblica officinalis*, *Bombax malabaricum*, etc., with high DBH ranges may be considered under threat from pioneer species such as *Lantana camara* and *Murraya koenigii*.

The remaining forests after deforestation need to be prioritised for conservation efforts, which may help in recovering AGB and enhancing the carbon pool in the existing forest (Gann et al., 2019). Already degraded sites should be selected instead of focusing on non-forest land to tackle desertification (Liu et al., 2020), utilising technologies such as drones and LiDAR (Deere et al., 2020). Multiple stakeholders and local communities should participate in reforestation projects.

Assisted natural regeneration could be applied by selectively planting missing species and clearing weeds to boost natural regeneration (FAO, 2019). The framework species approach may be followed by planting mixed species that shade out herbaceous weeds, which attract seed dispersal by animals. Selection of mixed species for plantation is important over monoculture (Brancalion and Chazdon, 2017). When natural regeneration is insufficient, tree plantation is necessary for forest restoration following the Nucleation approach of planting trees in small groups (Zahawi et al., 2013). Prioritisation should be given to native species while avoiding invasive species to achieve a high level of biodiversity with biomass. The key outcome of such plantations is to maximise functional diversity alongside natural diversity. The above conservation and management strategies are of utmost importance for biomass accumulation and biodiversity recovery after deforestation in the study area.

5. CONCLUSION

This research focused on carbon stock estimation due to deforestation in the subtropical Himalayas and revealed that CRI and VEG are the most effective indices, and the Green and Red edge bands of Sentinel 2A products are appropriate for biomass estimation in mixed forests. The best-fitting polynomial model was established between these indices and observed biomass. Therefore, a 12.04% loss in carbon stock might indicates significant ecological shifts in species due to potential consequences of deforestation, such as an increase in surface albedo contributing to local climate warming and altered rainfall patterns in the study area. Concurrently, shifts in vegetation composition may occur, with climax communities potentially being replaced by pioneer species. As such, urgent attention and prioritisation are required for conservation efforts in the study area. Moreover, this study has provided important baseline information for policymakers and established a framework for estimating carbon loss resulting from deforestation. We recommend proactive environmental management strategies that consider carbon sequestration dynamics in any developmental activities.

ACKNOWLEDGEMENTS

Authors thank Director, CSIR-IHBT, Palampur, India for providing his encouragement and facilities in carrying out this research. We are thankful to CCF, Hamirpur forest circle, Himachal Pradesh State Forest Department and staff members of Environmental Technology, CSIR-IHBT for lending their support during in the field work. Mr. Sunil Kumar, research scholar, AcSIR-CSIR-IHBT is acknowledged for his suggestions in the preparation of this manuscript. Author Vivek Dhiman acknowledges the University Grant Commission (UGC) (commencement No. 190510008590) for providing SRF fellowship.

Funding: This work is funded by University Grant Commission (UGC) (commencement No. 19051 0008590) of providing SRF Fellowship to author Vivek Dhiman. Also, this work was carried out under CSIR in-house funded project entitled “Assessing, monitoring, conserving Himalayan bio resources vis-a-vis understanding plant strategies and functions for its sustainable utilization (MLP-0206)”. This article represents CSIR-IHBT communication number 5333.

Declaration of Interest Statement: The authors declare no conflict of interests.

Data availability: The authors declare that all the raw, processed and analysed data related to the present study is with us and may be made available from the corresponding author upon reasonable requests, which is subject to further official formalities and approval from the competent authority.

REFERENCES

Aber JD, Federer CA. A generalized, lumped-parameter model of photosynthesis, evapotranspiration and net primary production in temperate and boreal forest ecosystems. Oecologia 1992;92:463-74.

Allouche O, Tsoar A, Kadmon R. Assessing the accuracy of species distribution models: Prevalence, kappa and the true skill statistic (TSS). Journal of Applied Ecology 2006; 43(6):1223-32.

Ali N, Saad M, Ali A, Ahmad N, Khan IA, Ullah H, et al. Assessment of aboveground biomass and carbon stock of subtropical pine forest of Pakistan. Journal of Forest Science 2023;69:287-304.

Astola H, Hame T, Sirro L, Molinier M, Kilpi J. Comparison of Sentinel-2 and Landsat 8 imagery for forest variable prediction in boreal region. Remote Sensing of Environment 2019; 15(223):257-73.

Baldocchi D, Falge E, Gu L, Olson R, Hollinger D, Running S, et al. FLUXNET: A new tool to study the temporal and spatial variability of ecosystem-scale carbon dioxide, water vapor, and energy flux densities. Bulletin of the American Meteorological Society 2001;82(11):2415-34.

Baret F, Guyot G. Potentials and limits of vegetation indices for LAI and APAR assessment. Remote Sensing of Environment 1991;35(2-3):161-73.

Bisleshna T, Sarkar BC, Pala NA, Gopal S, Sofi PA. Wood specific gravity of some tree species in sub-tropical humid climate of India. Indian Forester 2019;145(7):637-42.

Brancalion PH, Chazdon RL. Beyond hectares: Four principles to guide reforestation in the context of tropical forest and landscape restoration. Restoration Ecology 2017;25(4):491-6.

Broge NH, Leblanc E. Comparing prediction power and stability of broadband and hyperspectral vegetation indices for estimation of green leaf area index and canopy chlorophyll density. Remote Sensing of Environment 2001;76(2):156-72.

Brown S. Tropical forests and the global carbon cycle: The need for sustainable land-use patterns. Agriculture, Ecosystems and Environment 1993;46(1-4):31-44.

Castillo JA, Apan AA, Maraseni TN, Salmo III SG. Estimation and mapping of above-ground biomass of mangrove forests and their replacement land uses in the Philippines using Sentinel imagery. ISPRS Journal of Photogrammetry and Remote Sensing 2017;134:70-85.

Chaturvedi RK, Raghubanshi AS. Aboveground biomass estimation of small diameter woody species of tropical dry forest. New Forests 2013;44:509-19.

Chen L, Wang Y, Ren C, Zhang B, Wang Z. Assessment of multi-wavelength SAR and multispectral instrument data for forest aboveground biomass mapping using random forest kriging. Forest Ecology and Management 2019;447:12-25.

Chen JM. Evaluation of vegetation indices and a modified simple ratio for boreal applications. Canadian Journal of Remote Sensing 1996;22(3):229-42.

Chen L, Ren C, Zhang B, Wang Z, Xi Y. Estimation of forest above-ground biomass by geographically weighted regression and machine learning with sentinel imagery. Forests 2018;9(10):Article No. 582.

Chrysafis I, Mallinis G, Siachalou S, Patias P. Assessing the relationships between growing stock volume and Sentinel-2 imagery in a Mediterranean forest ecosystem. Remote Sensing Letters 2017;8(6):508-17.

Clevers JG, Gitelson AA. Remote estimation of crop and grass chlorophyll and nitrogen content using red-edge bands on Sentinel-2 and -3. International Journal of Applied Earth Observation and Geoinformation 2013;23:344-51.

Climate Funds Update (CFU). Climate Finance Thematic Briefing: REDD+ Finance. Washington, USA: Heinrich Boll Stiftung; 2020.

Deere NJ, Guillera-Arroita G, Swinfield T, Milodowski DT, Coomes DA, Bernard H, et al. Maximizing the value of forest restoration for tropical mammals by detecting three-dimensional habitat associations. Proceedings of the National Academy of Sciences 2020;117(42):26254-62.

Food and Agricultural Organization (FAO). Restoring Forest Landscapes through Assisted Natural Regeneration (ANR): A Practical Manual. Bangkok: Food and Agriculture Organization of the United Nations; 2019.

Farooq M, Rashid H. Spatio temporal change analysis of forest density in Doodhganga Forest range, Jammu and Kashmir. International Journal of Geomatics and Geosciences 2010; 1(2):132-40.

Fearnside PM. Wood density for estimating forest biomass in Brazilian Amazonia. Forest Ecology and Management 1997;90(1):59-87.

Gann GD, McDonald T, Walder B, Aronson J, Nelson CR, Jonson J, et al. International principles and standards for the practice of ecological restoration. Restoration Ecology 2019;27(S1):1-46.

Gitelson AA, Vina A, Arkebauer TJ, Rundquist DC, Keydan G, Leavitt B. Remote estimation of leaf area index and green leaf biomass in maize canopies. Geophysical Research Letters 2003;30(5):Article No. 1199.

Gitelson AA. Wide dynamic range vegetation index for remote quantification of biophysical characteristics of vegetation. Journal of Plant Physiology 2004;161(2):165-73.

Gitelson AA. Use of a green channel in remote sensing of global vegetation from EOSMODIS. Remote Sensing of Environment 1996;58:289-98.

Gitelson AA, Kaufman YJ, Stark R, Rundquist D. Novel algorithms for remote estimation of vegetation fraction. Remote Sensing of Environment 2002a;80(1):76-87.

Gitelson AA, Zur Y, Chivkunova OB, Merzlyak MN. Assessing carotenoid content in plant leaves with reflectance spectroscopy. Photochemistry and Photobiology 2002b; 75(3):272-81.

Goel NS, Qin W. Influences of canopy architecture on relationships between various vegetation indices and LAI and FPAR: A computer simulation. Remote Sensing Reviews 1994;10(4):309-47.

Haboudane D, Miller JR, Pattey E, Zarco-Tejada PJ, Strachan IB. Hyperspectral vegetation indices and novel algorithms for predicting green LAI of crop canopies: Modeling and validation in the context of precision agriculture. Remote Sensing of Environment 2004;90(3):337-52.

Houghton RA, Hall F, Goetz SJ. Importance of biomass in the global carbon cycle. Journal of Geophysical Research: Biogeosciences 2009;114:148-227.

Huete AR. A soil-adjusted vegetation index (SAVI). Remote Sensing of Environment 1988;25(3):295-309.

Hunt Jr ER, Daughtry CS, Eitel JU, Long DS. Remote sensing leaf chlorophyll content using a visible band index. Agronomy Journal 2011;103(4):1090-9.

The European Union and the World Agroforestry Centre (ICRAF). Wood Density Database [Internet]. 2007 [cited 2024 Jun 21]. Available from: https://apps.worldagroforestry.org/treedb/index.php?keyword=Timber.

Isbaex C, Coelho AM. The potential of Sentinel-2 Satellite Images for land-cover/land-use and forest biomass estimation: A review. In: Cristina GA, Sousa A, Malico I, editors. Forest Biomass - From Trees to Energy. IntechOpen; 2021. p. 2-25.

Intergovernmental Panel on Climate Change (IPCC). IPCC National Greenhouse Gas Inventories Programme: Good Practice Guidance for Land Use, Land-Use Change and Forestry. Japan: Institute for Global Environmental Strategies; 2003.

Intergovernmental Panel on Climate Change (IPCC). IPCC Guidelines for National Greenhouse Gas Inventories: Volume 1-5. Hayama, Japan: Institute for Global Environmental Strategies; 2006.

International Hydropower Association (IHA). Hydropower: the facts [Internet]. 2024 [cited 2024 Jun 21]. Available from: https://www.hydropower.org/net-zero.

Vashum KT, Jayakumar S. Methods to estimate above-ground biomass and carbon stock in natural forests: A review. Journal of Ecosystem and Ecography 2012;2(4):1-7.

Joshi VC, Negi VS, Bisht D, Sundriyal RC, Arya D. Tree biomass and carbon stock assessment of subtropical and temperate forests in the Central Himalaya, India. Trees, Forests and People 2021;6:Article No. 100147.

Kataoka T, Kaneko T, Okamoto H, Hata S. Crop growth estimation system using machine vision. Proceeding of the IEEE/ASME International Conference on Advanced Intelligent Mechatronics; 2003 July 20-24; Kobe, Japan; 2003.

Ke W, Zhangquan S, RenChao W. Effects of nitrogen nutrition on the spectral reflectance characteristics of rice leaf and canopy. Journal of Zhejiang Agricultural University 1998;24(1);93-7.

Khan MN, Tan Y, Gul AA, Abbas S, Wang J. Forest aboveground biomass estimation and inventory: Evaluating remote sensing-based approaches. Forests 2024;15(6):Article No. 1055.

Kuyah S, Dietz J, Muthuri C, Jamnadass R, Mwangi P, Coe R, et al. Allometric equations for estimating biomass in agricultural landscapes: II. Belowground biomass. Agriculture, Ecosystems and Environment 2012;158:225-34.

Lawrence D, Coe M, Walker W, Verchot L, Vandecar K. The unseen effects of deforestation: Biophysical effects on climate. Frontiers in Forests and Global Change 2022;5:Article No. 756115.

Levia DF, Carlyle-Moses D, Tanaka T. Forest Hydrology and Biogeochemistry: Synthesis of Past Research and Future Directions. Springer; 2011.

Lewis CD. Industrial and Business Forecasting Methods: A Practical Guide to Exponential Smoothing and Curve Fitting. Boston, London: Butterworth Scientific; 1982.

Liu HQ, Huete A. A feedback-based modification of the NDVI to minimize canopy background and atmospheric noise. IEEE

Transactions on Geoscience and Remote Sensing 1995; 33:457-65.

Liu Q, Zhang Q, Yan Y, Zhang X, Niu J, Svenning JC. Ecological restoration is the dominant driver of the recent reversal of desertification in the Mu Us Desert (China). Journal of Cleaner Production 2020;268:Article No. 122241.

Lingbing L, Jing SH. The potential carbon losses estimation with remote sensing-based data: Case study in Nova Vida Ranch, Rondonia, Brazil. Proceedings of the International Archives of the Photogrammetry, Remote Sensing and Spatial Information Sciences; 2022 June 6-11; Nice, France; 2022.

Lousada S, Cabezas J, Castanho RA, Gomez JM. Land-use changes in insular urban territories: A retrospective analysis from 1990 to 2018. The case of Madeira Island-Ribeira Brava. Sustainability 2022;14(24):Article No. 16839.

Lu D, Chen Q, Wang G, Liu L, Li G, Moran E. A survey of remote sensing-based aboveground biomass estimation methods in forest ecosystems. International Journal of Digital Earth 2016;9(1):63-105.

Lu D, Batistella M, Moran E. Satellite estimation of aboveground biomass and impacts of forest stand structure. Photogrammetric Engineering and Remote Sensing 2005; 71(8):967-74.

Lu D, Chen Q, Wang G, Moran E, Batistella M, Zhang M, et al. Aboveground forest biomass estimation with Landsat and LiDAR data and uncertainty analysis of the estimates. International Journal of Forestry Research 2012;2012:Article No. 436537.

Luo H, Gao X, Liu Z, Liu W, Li Y, Meng X, et al. Real-time characterization model of carbon emissions based on land-use status: A case study of Xi'an City, China. Journal of Cleaner Production 2024;434:Article No. 140069.

Makridakis S, Wheelwright SC, Hyndman RJ. Forecasting Methods and Applications. New York: John Wiley and Sons; 2008.

Marchant JA, Onyango CM. Shadow-invariant classification for scenes illuminated by daylight. Journal of the Optical Society of America 2000;17(11):1952-61.

Meyer GE, Neto JC. Verification of color vegetation indices for automated crop imaging applications. Computers and Electronics in Agriculture 2008;63(2):282-93.

Mitchard ET, Saatchi SS, Baccini A, Asner GP, Goetz SJ, Harris NL, et al. Uncertainty in the spatial distribution of tropical forest biomass: A comparison of pan-tropical maps. Carbon Balance and Management 2013;8:1-3.

Moisa MB, Dejene IN, Deribew KT, Gurmessa MM, Gemeda DO. Impacts of forest cover change on carbon stock, carbon emission and land surface temperature in Sor watershed, Baro Akobo Basin, Western Ethiopia. Journal of Water and Climate Change 2023;14(8):2842-60.

Mukuralinda A, Kuyah S, Ruzibiza M, Ndoli A, Nabahungu NL, Muthuri C. Allometric equations, wood density and partitioning of aboveground biomass in the arboretum of Ruhande, Rwanda. Trees, Forests and People 2021;3:Article No. 100050.

Mutanga O, Skidmore AK. Narrow band vegetation indices overcome the saturation problem in biomass estimation. International Journal of Remote Sensing 2004;25(19):3999-4014.

Nadrowski K, Wirth C, Scherer-Lorenzen M. Is forest diversity driving ecosystem function and service. Current Opinion in Environmental Sustainability 2010;2(1-2):75-9.

Nandy S, Singh R, Ghosh S, Watham T, Kushwaha SP, Kumar AS, et al. Neural network-based modelling for forest biomass assessment. Carbon Management 2017;8(4):305-17.

Nath AJ, Tiwari BK, Sileshi GW, Sahoo UK, Brahma B, Deb S, et al. Allometric models for estimation of forest biomass in North East India. Forests 2019;10(2):Article No. 103.

Navar J. Allometric equations for tree species and carbon stocks for forests of northwestern Mexico. Forest Ecology and Management 2009;257(2):427-34.

Ostertagova E. Modelling using polynomial regression. Procedia Engineering 2012;48:500-6.

Pandit S, Tsuyuki S, Dube T. Estimating above-ground biomass in sub-tropical buffer zone community forests, Nepal, using Sentinel 2 data. Remote Sensing 2018;10(4):Article No. 601.

Pearson T, Wolker S, Brown S. Source Book for Land Use, Land Use Change and Forestry Projects. USA: Winrock International and the Bio Carbon Fund, World Bank; 2005.

Pearson RL, Miller LD. Remote mapping of standing crop biomass for estimation of the productivity of the shortgrass prairie, Pawnee National Grasslands, Colorado. Proceedings of the 8th International Symposium on Remote Sensing of Environment; 1972 Oct 2-6; Ann Arbor, Michigan: 1972.

Pearson TR, Brown S, Murray L, Sidman G. Greenhouse gas emissions from tropical forest degradation: An underestimated source. Carbon Balance and Management 2017;12:1-11.

Peres CA, Barlow J, Laurance WF. Detecting anthropogenic disturbance in tropical forests. Trends in Ecology and Evolution 2006;21(5):227-9.

Pitman AJ, Avila FB, Abramowitz G, Wang YP, Phipps SJ, de Noblet-Ducoudre N. Importance of background climate in determining impact of land-cover change on regional climate. Nature Climate Change 2011;1(9):472-5.

Rawat YS, Singh JS. Structure and function of oak forests in central Himalaya. I. Dry matter dynamics. Annals of Botany 1988;62(4):397-411.

Reyes G. Wood Densities of Tropical Tree Species. US Department of Agriculture, Forest Service: Southern Forest Experiment Station; 1992.

Rondeaux G, Steven M, Baret F. Optimization of soil-adjusted vegetation indices. Remote Sensing of Environment 1996; 55(2):95-107.

Rouse JW, Haas RH, Schell JA, Deering DW. Monitoring vegetation systems in the Great Plains with ERTS. NASA Special Publication 1974;351(1):Article No. 309.

Scott CE, Monks SA, Spracklen DV, Arnold SR, Forster PM, Rap A, et al. Impact on short-lived climate forcers increases projected warming due to deforestation. Nature Communications 2018;9(1):Article No. 157.

Shannon CE, Weaver W. The Mathematical Theory of Communication. Urbana, IL: University of Illinois Press; 1949.

Sheikh MA, Kumar M, Bhat JA. Wood specific gravity of some tree species in the Garhwal Himalayas, India. Forestry Studies in China 2011;13:225-30.

Simpson E. Measurement of diversity. Nature 1949;163:Article No. 688.

Social Impact Assessment Unit (SIAU) Social Impact Assessment Study for the Purpose of Proposed Land Acquisition in District Hamirpur and Kangra for Dhaulasidh Hydroelectric Project (66 MW) [Internet]. 2019 [cited 2024 Jun 21]. Available from: https://sjvnindia.com/UploadFiles/GroupLinks/127_1_SIA_Dhaulasidh_Eng.pdf.

Slonecker T, Haack B, Price S. Spectroscopic analysis of arsenic uptake in Pteris ferns. Remote Sensing 2009;1(4):644-75.

Timothy D, Onisimo M, Riyad I. Quantifying aboveground biomass in African environments: A review of the trade-offs between sensor estimation accuracy and costs. Tropical Ecology 2016;57(3):393-405.

United Nations Framework Convention on Climate Change (UNFCCC). Informal Meeting of Experts on Methodological Issues relating to Reducing Emissions from Forest Degradation in Developing Countries. Bonn, Germany: UNFCCC; 2008.

United Nations Framework Convention on Climate Change (UNFCCC). Report of the Conference of the Parties on its 15th session. Copenhagen, Denmark: UNFCCC; 2009.

West GB, Brown JH, Enquist BJ. A general model for the structure and allometry of plant vascular systems. Nature 1999;400:664-7.

Woebbecke DM, Meyer GE, Von Bargen K, Mortensen DA. Color indices for weed identification under various soil, residue, and lighting conditions. Transactions of the American Society of Agricultural and Biological Engineers 1995;38(1):259-69.

Yan H, Wang S, Dai J, Wang J, Chen J, Shugart HH. Forest greening increases land surface albedo during the main growing period between 2002 and 2019 in China. Journal of Geophysical Research: Atmospheres 2021;126(6): e2020JD033582.

Yan D, Liu C, Li P. Effect of carbon emissions and the driving mechanism of economic growth target setting: An empirical study of provincial data in China. Journal of Cleaner Production 2023;415:Article No. 137721.

Zahawi RA, Holl KD, Cole RJ, Reid JL. Testing applied nucleation as a strategy to facilitate tropical forest recovery. Journal of Applied Ecology 2013;50(1):88-96.

Zhang T, Su J, Liu C, Chen WH, Liu H, Liu G. Band selection in sentinel-2 satellite for agriculture applications. Proceedings of the 23rd International Conference on Automation and Computing (ICAC); 2017 Sep 7; IEEE; 2017. p. 1-6.

Zhang X, Zhang D. Urban carbon emission scenario prediction and multi-objective land use optimization strategy under carbon emission constraints. Journal of Cleaner Production 2023; 430:Article No. 139684.

Zhou G, Peng C, Li Y, Liu S, Zhang Q, Tang X, et al. A climate change-induced threat to the ecological resilience of a subtropical monsoon evergreen broad-leaved forest in Southern China. Global Change Biology 2013;19(4):1197-210.

Zwane TT, Udimal TB, Pakmoni L. Examining the drivers of agricultural carbon emissions in Africa: An application of FMOLS and DOLS approaches. Environmental Science and Pollution Research 2023;(19):56542-57.